Modulated Electron Cyclotron Drift Instability in a High-Power Pulsed Magnetron Discharge

Sedina Tsikata*
ICARE, UPR 3021 CNRS, 1C Avenue de la Recherche Scientifique, 45071 Orléans, France

Tiberiu Minea
LPGP, UMR 8578 CNRS, Université Paris-Sud XI, 91405 Orsay Cedex, France
(Received 13 February 2015; published 8 May 2015)

The electron cyclotron drift instability, implicated in electron heating and anomalous transport, is detected in the plasma of a planar magnetron. Electron density fluctuations associated with the mode are identified via an adapted coherent Thomson scattering diagnostic, under direct current and high-power pulsed magnetron operation. Time-resolved analysis of the mode amplitude reveals that the instability, found at MHz frequencies and millimeter scales, also exhibits a kHz-scale modulation consistent with the observation of larger-scale plasma density nonuniformities, such as the rotating spoke. Sharply collimated axial fluctuations observed at the magnetron axis are consistent with the presence of escaping electrons in a region where the magnetic and electric fields are antiparallel. These results distinguish aspects of magnetron physics from other plasma sources of similar geometry, such as the Hall thruster, and broaden the scope of instabilities which may be considered to dictate magnetron plasma features.

DOI: 10.1103/PhysRevLett.114.185001 PACS numbers: 52.35.-g, 52.25.Os, 84.40.Fe

Crossed-field plasma discharges, such as Hall thrusters and planar magnetrons, owe their operation to the confinement of electrons which execute a fast (on the order of 10^5–10^6 m/s) azimuthal drift. This drift, in the region of the plasma with orthogonal electric and magnetic fields, makes possible the maintenance of a large electric field for ion acceleration and a sufficiently high ionizing collision frequency between electrons and neutrals, even at very low pressure. These characteristics make such devices well suited to different applications: for the Hall thruster, highly efficient electric propulsion, and for the magnetron, plasma-assisted deposition with an enhanced sputtering efficiency.

The azimuthal drift also gives rise to plasma waves such as the electron cyclotron drift instability (ECDI), driven by the difference in electron and ion velocities. It has been studied in the past, in the context of collisionless shocks and θ-pinch machines, to account for anomalous cross-field particle transport [1–3]. In recent years, theoretical analyses and numerical simulations have revealed that the ECDI also plays a role in enhancing electron current in the Hall thruster plasma [4–6], where it is associated with a broadening of the electron energy distribution functions parallel and perpendicular to the applied magnetic field. The mechanism for heating, while still under investigation, is thought to be analogous to ion heating by a lower hybrid wave, first described by Karney [7].

Experimental evidence for the presence of this instability in the thruster plasma was provided through the development and implementation of a coherent Thomson scattering diagnostic known as PRopulsion Analysis eXperiments via Infrared Scattering [8]. In this Letter, the diagnostic implementation has been extended to the study of unique features of a high-impulse pulsed magnetron sputtering (HIPIMS) plasma.

From analysis of the dispersion relation for electrostatic waves in a plasma with magnetized electrons and unmagnetized ions [3,4], the ECDI is expected to be excited in the vicinity of electron cyclotron resonances, i.e., for discrete values of azimuthal wave number k_y

$$k_y V_d = n\omega_{ce}, \tag{1}$$

where V_d is the azimuthal electron drift velocity, ω_{ce} the electron cyclotron angular frequency, and n an integer 1 or greater. Based on the parameters typical for experiments described in this Letter (electric field magnitude $\approx 10^4$ V/m, magnetic field magnitude of 8.8 mT at the measurement position), excited modes in the magnetron plasma are expected at wave number values which correspond to length scales on the order of a millimeter and below. However, the expected cyclotron resonances can be smoothed, resulting in an observed mode dispersion relation which is nondiscrete [9].

To rapidly illustrate this, linear kinetic theory results for typical magnetron parameters (given in the figure caption) for an argon plasma are shown in Fig. 1. The dashed line shows the dispersion relation (f, k_y) when the axial (k_x) and radial (k_z) wave numbers are set to zero. The mode is excited at discrete k_y values. The full line shows, on the other hand, the dispersion relation obtained for $k_x = 0$ and $k_z = 1000$ rad/m. The inclusion of the radial wave vector component (a more realistic representation of the mode

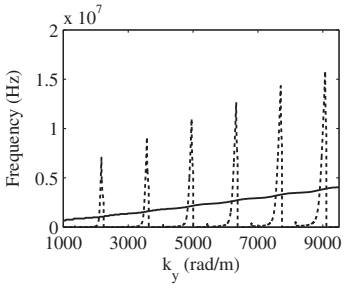

FIG. 1. Dispersion relation results from linear kinetic theory, showing ECDI resonances (dashed line) and smoothed resonances (solid line). In this example, $n_e = 10^{18}$ m^{-3}, $V_{te}/V_d = 0.64$, and $\omega_{ce}/\omega_{pe} = 0.027.n_e$, V_{te} and ω_{pe} are the electron density, electron thermal velocity, and electron plasma frequency, respectively.

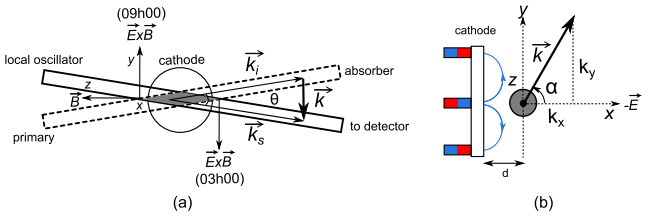

FIG. 2 (color online). (a) Definition of observation wave vector $\vec{k}$ from the incident $\vec{k}_i$ and scattered wave vectors $\vec{k}_s$. The gray region is the observation volume formed by the local oscillator and primary beam intersection. (b) A view of the observation wave vector orientation angle α and positioning at a distance d from the cathode surface. Magnets behind the cathode and typical magnetic field lines (in blue) are shown.

propagation) smoothes the resonances. The resulting dispersion relation is linear and the corresponding mode group velocity is 2.5 km/s.

In our experiment, correlated electron density fluctuations are measured at length scales and orientations which are set using two laser beams. The plasma-scattered signal is rendered measurable by the use of a heterodyne detection scheme. This scheme involves interference of the plasma-scattered radiation with a reference (local oscillator) beam shifted in frequency with respect to the main (primary) beam. This primary beam is used to increase the scattered signal amplitude to a measurable level and define the properties of the observation wave vector $\vec{k}$ (magnitude and directivity) relative to the local oscillator. The diagnostic uses a 10.6 μm CO_2 continuous laser of about 40 W power (with 1% of the initial power used to construct the local oscillator). The beam waist in the observation region is 3.6 mm.

The planar magnetron used in experiments is operated with a 10 cm-diameter titanium cathode and run in dc and pulsed excitation regimes with argon as a working gas; a detailed description of the source and chamber is provided elsewhere [10]. The magnetic field is radial and is set using concentric permanent magnets (a cylindrical magnet at the cathode center and an annular magnet at the outer edge of the cathode). At the center of the cathode, the magnetic field is normal to the cathode surface [Fig. 2(b)].

The following coordinate system is used. As shown in Fig. 2, x is the horizontal axis, pointing outwards perpendicular to the cathode along $-\vec{E}$, z is aligned with $\vec{B}$, with the magnetic field directed radially outwards, and y is the vertical axis pointing in the same direction as the $\vec{E}\times\vec{B}$ drift at the 09h00 position on the cathode. Observations are performed at a fixed arbitrary axial distance d of 14 mm from the cathode surface, probing the plasma volume situated along the cathode center.

The diagnostic allows the magnitude of $\vec{k}$ and its orientation in the $(\vec{E}, \vec{E}\times\vec{B})$ plane to be varied. α increases from a value of 0° on the x axis in the anticlockwise direction. To vary α, on the bench, the primary beam is directed onto a pair of mirrors mounted on a rotation stage. The stage is manually rotated (with respect to a fixed local oscillator) such that the resulting primary beam angle in the $(\vec{E}, \vec{E}\times\vec{B})$ plane in front of the cathode changes. The observation wave numbers used in the following experiments range from about 5500 to 9000 rad/m, i.e., observation length scales between 1.14 and 0.70 mm. The angle θ, between the local oscillator and primary beams, is a few milliradians in experiments, with the observation volume length consequently traversing the entire cathode. For the sake of visibility, θ is not to scale in Fig. 2.

The signal recovered from the detector is the time series of two channels in phase quadrature which are used to reconstruct the complex scattered signal. These signals are recorded using a 14-bit GaGe® acquisition card at a frequency of 100 MHz and a 6.5×10^6 sample depth per channel. In the pulsed regimes, the start of signal acquisition triggers the start of plasma pulsing within a gate of 65 ms (the scattered signal acquisition duration). Simultaneous recordings of the discharge current I_d and discharge voltage U_d are triggered on an oscilloscope.

To improve the signal to noise ratio in HIPIMS excitation regimes, fast Fourier transform (FFT) analysis is performed only on segments of the scattered signal coinciding with periods during which the plasma is present. These spectra are then averaged.

Figure 3 shows the fast Fourier transform of the complex signal time series in two cases for a HIPIMS regime. Pulses are generated with a 100 μs width and period of 3 ms.

In this figure, the black line corresponds to a spectrum obtained when only the local oscillator crosses the plasma (the photonic noise signal). When the primary beam is allowed to traverse the plasma (necessary for defining the observation wave vector and for signal detection), the profile obtained is that shown on the blue line. Broad frequency peaks associated with the scattered signal are visible around ±1 MHz.

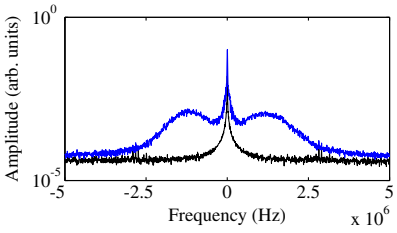

FIG. 3 (color online). FFT of signal time series for a pulsed-operation experiment. Broad frequency peaks around ± 1 MHz are visible on the blue line. The black line is a plot of the photonic noise signal. HIPIMS: peak $U_d = 504$ V, peak $I_d = 8.6$ A, $P = 15$ mTorr; $\alpha = 100°$, $k = 5600$ rad/m.

On the blue line [recorded at a near-azimuthal observation angle α of 100°, see Fig. 2(b)], the positive peak corresponds to an observation wave vector aligned with the direction of the azimuthal drift. The main azimuthal electron drift is clockwise, meaning that this peak then corresponds to the 09h00 position on the cathode, indicated in Fig. 2(a) (facing the cathode). The negative peak corresponds to the observation of fluctuations at the 03h00 channel, where the main azimuthal drift is now antiparallel to the observation wave vector.

Additional spectra [(i) detector closed and (ii) no plasma, local oscillator and primary beams present] are also used to calculate a frequency spectrum which gives an absolute measure of the amplitude of the scattered signal [11]. This spectrum is scaled against several experiment parameters including the laser power, beam waist, and detector efficiency, and is referred to as the dynamic form factor $S(k, \omega)$ (units of s^{-1}). $S(k, \omega)$ is integrated over the frequency range in which the signal of interest is present to give the unitless, absolute form factor $S(k)$ describing the intensity of the density fluctuations at a given wave number and frequency.

The observation length scale is varied and the positive signal peak frequencies at each wave number value are determined to construct the mode dispersion relation. Typical results are shown in Fig. 4 for different dc and HIPIMS excitation regimes. The frequencies shown correspond to the mean peak frequencies deduced from a Gaussian fit to the normalized signal profiles at the different wave numbers. Experimental conditions are given in the figure caption, with the HIPIMS experiment performed with a pulse period and width of 16 ms and 400 μs, respectively. The observation angles for both experiments are near the azimuthal direction.

A best-fit line through the points shown on Fig. 4 for the dc and HIPIMS experiments gives mode group velocities on the same order (respectively, 1.93 and 1.68 km/s) as those observed in a Hall thruster [8]. Error bar lengths shown in Fig. 4 correspond to the Gaussian peak widths.

The instability propagates azimuthally, however, it is visible within a broad angular range in the $(\vec{E}, \vec{E} \times \vec{B})$ plane, as illustrated by Fig. 5.

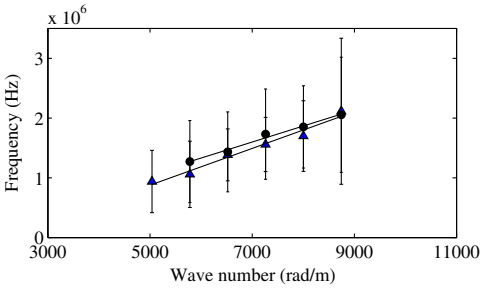

FIG. 4 (color online). Examples of the azimuthal mode dispersion relations, determined in dc (triangles) and HIPIMS (circles) regimes. dc: $U_d = 388$ V, $I_d = 0.5$ A, $P = 22.5$ mTorr; $\alpha = 85°$ HIPIMS: peak $U_d = 575$ V, peak $I_d = 22$ A, $P = 15$ mTorr; $\alpha = 100°$.

Figure 5 shows the results of an experiment in which the wave vector orientation (angle α) is varied over an angular range exceeding [0°, 90°], with the point O coinciding with the cathode center. For each angular position, a signal frequency peak is identified and integrated to give $S(k)$, shown in Fig. 5(a). The length of the arrows indicates the $S(k)$ magnitude. Arrows in red denote negative frequency peaks, while arrows in blue denote positive frequency peaks. Around 0°, the appearance of positive frequency peaks alone shows that density fluctuations propagate axially away from the cathode. Around 90°, both positive and negative frequency peaks are identifiable for the same angles. This is because the 09h00 and 03h00 azimuthal positions are visible simultaneously, as explained earlier (Fig. 3). The highest mode amplitude is observed at a certain inclination towards the cathode ($\alpha = 100°$), a result similar to that found on a Hall thruster [12].

Figure 5(a) shows one point around the axial direction ($\alpha = 5°$) with a static form factor amplitude about twice that measured at neighboring angles. The unexpectedly large signal at this angle, and its narrow angular restriction, point to the observation of escaping electrons at the cathode center. At the center of the cathode plasma, where the electric and magnetic fields are antiparallel, the electrons are not trapped and can flow freely away from the cathode surface. The observation of this signal peak at 5°, rather

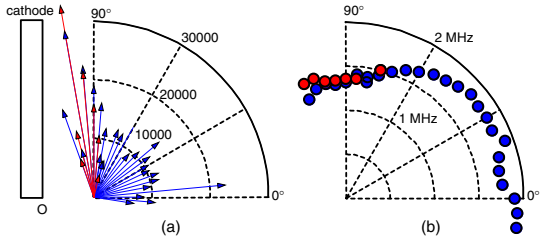

FIG. 5 (color online). Variation in (a) mode amplitude and (b) frequency with orientation angle α in the $(\vec{E}, \vec{E} \times \vec{B})$ plane [see Fig. 2(b)]. O represents the center of the cathode. dc: $U_d = 370$ V, $I_d = 0.4$ A; $k = 5600$ rad/m.

than exactly at 0°, may be attributed to a slight error in the angular referencing of the beams. The apparent collimation of the fluctuations about an angle normal to the cathode is in sharp contrast to observations made on a Hall thruster, where fluctuation amplitudes around 0° trace a Gaussian distribution with a full width of over 50° [13]. This key difference between the two devices arises because of the presence of plasma in the central region of the magnetron where $\vec{E}$ and $\vec{B}$ are antiparallel (unlike in the annular Hall thruster chamber). The relation between the observed axial density fluctuations and larger-scale electron flares observed by other authors [14] merits further investigation.

The density normalization applied to the signal is the same at every angle (a chosen value of 10^{18} m^3) because, while α is varied, the actual position of the observation volume does not change. The observed $S(k)$ signal peak at 5° corresponds to a real increase in the mode fluctuation intensity (unbiased by the effect of the density) associated with the escaping electrons.

Frequencies of the mode at different angles are shown in Fig. 5(b). The positive and negative peaks remain symmetric in frequency (±1.5 MHz) near the azimuthal direction. Frequencies observed in the axial direction are of similar magnitudes.

HIPIMS operation of the magnetron, with simultaneous acquisition of the scattered signal, can provide an opportunity for the evolution of the electron density fluctuations within a single pulse to be studied (Fig. 6). Here, we consider plasma conditions identical to those used for the signal plot shown in blue in Fig. 3. Within the 65 ms signal acquisition window, 22 pulses are generated; Fig. 6 concerns pulse 3 only.

The spectrogram for a segment of the signal around this pulse is determined and shown in Fig. 6(b). The continuous signal band at frequencies of 200 kHz and below, visible on Fig. 6(b), is largely attributable to diffraction. The scattered signal of interest is identifiable over a range from about 0.2 to 3 MHz; this breadth in frequency is reflected in the spectral width of the signal shown in Fig. 3. The color levels of Fig. 6(b) are given by the product $10\log_{10}|P_s|$, where P_s is the power spectral density.

Figure 6(b) shows a very interesting feature: low-frequency modulation of the MHz-frequency signal within the pulse which is not evident from the time-averaged FFT analysis. To highlight this, the time evolution of the power spectral density at 1 MHz is examined. This variation is shown in Fig. 6(c). A low-frequency modulation of the mode amplitude at about 120 kHz is clear; a similar modulation is also identifiable when other pulses are analyzed.

One likely reason for the oscillation in mode amplitude is the traversal of the observation volume by regions of alternating high and low electron densities. Each crossing of the observation volume by a region of plasma with higher density than the mean electron density would

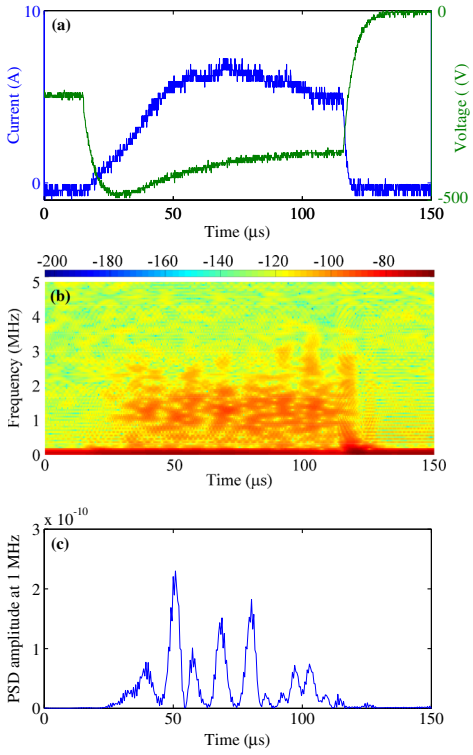

FIG. 6 (color online). Pulse characteristics and mode features. (a) Current (blue) and discharge voltage (green) profiles within the chosen pulse, (b) spectrogram of the scattered signal within the pulse envelope [amplitudes equal to $10\log_{10}|P_s|$, where P_s is the power spectral density (PSD)], and (c) time variation of power spectral density at 1 MHz, showing low-frequency periodicity. HIPIMS: peak $U_d = 494$ V, peak $I_d = 7$ A, $P = 15$ mTorr; $\alpha = 100°$, $k = 5600$ rad/m.

increase the scattered signal intensity proportionally. Such conditions could well be created by the crossing of the observation region by rotating spokes.

Here, we draw a distinction between the results from this Letter and the numerous other studies on azimuthal instabilities in the magnetron. The mode detected via probes by Lundin *et al.* [15] and Winter *et al.* [16] and described as the modified two-stream instability is a large-wavelength (several cm) drift instability with MHz frequencies, similar to that detected in the Hall thruster context by Lazurenko *et al.* [17]. Azimuthal large scale structures with kHz periodicities, described as being driven by ionization and density gradients, have been identified by other authors ([14], [18], [19], among others). The mode identified in this Letter is driven neither by ionization nor by gradients, and its frequency and length scale ranges differ from those found in the aforementioned studies. The instability is also not a pure ion acoustic wave [20]; it arises, instead, when Doppler-shifted Bernstein waves couple to ion acoustic waves [3].

This Letter provides evidence (via the low frequency modulation of the small-scale, MHz signal) of the presence

of electric fields within large-scale structures. This goes a step beyond the simultaneous observations of kHz and MHz features found in Refs. [16] and [21] and is only rendered possible by the access to millimetric and sub-millimetric length scales our diagnostic provides. These results could provide experimental backing for recent ideas of Brenning and colleagues involving the creation of short-scale internal electric fields in spokes [22].

When considered in the context of studies which have so far been performed on instabilities on the magnetron, our study brings to light (i) the presence of a MHz, mm-scale instability, distinct from those previously described in magnetron plasmas, identified as the ECDI, (ii) the presence of collimated, axial electron density fluctuations at electron Larmor radius scales, and (iii) the presence of short-scale electric fields within large-scale structures of kHz periodicity. Investigations of the wave number and frequency matching conditions, as a means of understanding the nonlinear coupling across different scales, will be made in future work.

The authors are grateful to the Réseau Plasmas Froids for partial funding of this research, and to A. Héron and O. Antonin.

*sedina.tsikata@cnrs-orleans.fr

[1] D. W. Forslund, R. L. Morse, and C. W. Nielson, Phys. Rev. Lett. **25**, 1266 (1970).
[2] M. Lampe, W. M. Manheimer, J. B. McBride, J. H. Orens, R. Shanny, and R. N. Sudan, Phys. Rev. Lett. **26**, 1221 (1971).
[3] S. P. Gary and J. J. Sanderson, J. Plasma Phys. **4**, 739 (1970).
[4] J-C. Adam, A. Héron, and G. Laval, Phys. Plasmas **11**, 295 (2004).
[5] A. Ducrocq, J-C. Adam, A. Héron, and G. Laval, Phys. Plasmas **13**, 102111 (2006).
[6] A. Héron and J-C. Adam, Phys. Plasmas **20**, 082313 (2013).
[7] C. F. F. Karney, Phys. Fluids **21**, 1584 (1978).
[8] S. Tsikata, N. Lemoine, V. Pisarev, and D. Grésillon, Phys. Plasmas **16**, 033506 (2009).
[9] J. Cavalier, N. Lemoine, G. Bonhomme, S. Tsikata, C. Honoré, and D. Grésillon, Phys. Plasmas **20**, 082107 (2013).
[10] C. Vitelaru, L. de Poucques, T. M. Minea, and G. Popa, J. Appl. Phys. **109**, 053307 (2011).
[11] D. Grésillon, C. Stern, A. Hémon, A. Truc, T. Lehner, J. Olivain, A. Quéméneur, F. Gervais, and Y. Lapierre, Phys. Scr. **T2B**, 459 (1982).
[12] S. Tsikata, C. Honoré, N. Lemoine, and D. M. Grésillon, Phys. Plasmas **17**, 112110 (2010).
[13] S. Tsikata, J. Cavalier, A. Héron, C. Honoré, N. Lemoine, D. Grésillon, and D. Coulette, Phys. Plasmas **21**, 072116 (2014).
[14] A. Anders, P. Ni, and A. Rauch, J. Appl. Phys. **111**, 053304 (2012).
[15] D. Lundin, U. Helmersson, S. Kirkpatrick, S. Rohde, and N. Brenning, Plasma Sources Sci. Technol. **17**, 025007 (2008).
[16] J. Winter, A. Hecimovic, T. de los Arcos, M. Boke, and V. Schulz von de Gathen, J. Phys. D **46**, 084007 (2013).
[17] A. Lazurenko, G. Coduti, S. Mazouffre, and G. Bonhomme, Phys. Plasmas **15**, 034502 (2008).
[18] A. P. Ehiasarian, A. Hecimovic, T. de los Arcos, R. New, V. Schulz von der Gathen, M. Böke, and J. Winter, Appl. Phys. Lett. **100**, 114101 (2012).
[19] E. Martines, R. Cavazzana, G. Serianni, M. Spolaore, L. Tramontin, M. Zuin, and V. Antoni, Phys. Plasmas **8**, 3042 (2001).
[20] T. E. Sheridan and J. Goree, J. Vac. Sci. Technol. A **7**, 1014 (1989).
[21] I. Lin and W. Ming-Shing, J. Appl. Phys. **62**, 4077 (1987).
[22] N. Brenning, D. Lundin, T. Minea, C. Costin, and C. Vitelaru, J. Phys. D **46**, 084005 (2013).